Fatigue of LIGA Ni Micro-Electro-Mechanical System Thin Films

Y. YANG, S. ALLAMEH, J. LOU, B. IMASOGIE, B.L. BOYCE, and W.O. SOBOYEJO

This article presents the results of an experimental study of the mechanisms of fatigue in 270-μm-thick LIGA (lithographic, galvanoformung, abformung) Ni micro-electro-mechanical systems (MEMS) thin films with columnar microstructure. Stress-life behavior is compared with the previously reported data for LIGA Ni MEMS films and bulk Ni. The LIGA Ni thin films are shown to have comparable fatigue lives to bulk annealed Ni. The underlying mechanisms of fatigue crack growth are elucidated *via* scanning electron and focused ion beam (FIB) microscopy. Stress-driven recrystallization was revealed near the fatigue crack-tip using FIB microscopy. Microvoids were also found to form and coalesce in the recrystallized grains. This led to subsequent fatigue crack growth at the microscopic and macroscopic scales. The crack profiles revealed that fatigue crack growth was retarded by crack deflection and branching. The implications of the results are then discussed for the analyses of fatigue in nickel MEMS structures.

DOI: 10.1007/s11661-007-9246-y
© The Minerals, Metals & Materials Society and ASM International 2007

I. INTRODUCTION

IN recent years, LIGA (lithographic, galvanoformung, abformung) processing, which is the German acronym for electrodeposition into PMMA (polymethylmethacrylate) molds has been used to fabricate Ni microelectromechanical system (MEMS) thin films.[1–34] These have emerged as candidate materials for applications in larger and thicker MEMS devices (>20-μm thick) with high aspect ratios.[17] The potential applications include the following: microswitches, microgears, and linkage mechanisms, micromotors, and accelerometers for the deployment of airbags.[29]

In many of these potential applications, fatigue failure can occur at stress ranges that are significantly below the measured strengths under monotonic loading.[30] However, until recently,[31] it has been difficult to diagnose fatigue failure in LIGA Ni MEMS structures, such as Ni MEMS accelerometers.[32,33] This was due largely to the limited number of fractographic studies of fatigue in LIGA Ni MEMS thin films/structures at the time of diagnoses.

Recent efforts have been made to study the fatigue mechanisms in LIGA Ni MEMS thin films.[4,5,8,31,34] The initial work was done by Hemker *et al.*[8] and Cho *et al.*,[4,5] who measured the stress-life behavior of LIGA Ni MEMS thin films and compared their results with previously reported data for annealed and wrought bulk Ni. Most recently, Allameh *et al.*[31] have studied the effects of specimen thickness on the stress-life behavior and the fatigue fracture modes in LIGA Ni MEMS structures. Furthermore, Boyce *et al.*[34] have suggested that fatigue cracks nucleate from an oxide film that forms on the surfaces of slip bands that are induced on the surfaces of cyclically deformed LIGA Ni MEMS thin films. However, an integrated understanding of the mechanisms of fatigue crack nucleation and growth in LIGA Ni MEMS structures is yet to emerge.

This article presents the results of an experimental study of the mechanisms of fatigue crack nucleation and growth in LIGA Ni MEMS thin films with columnar microstructures and a top layer of nanoscale equiaxed grains. Following a brief description of material processing and microstructure in Section II, the experimental techniques are described in Section III. The underlying mechanisms of fatigue crack nucleation and propagation are then presented in Section IV. The implications of the current results are discussed in Section V, before presenting the salient conclusions arising from this work in Section VI.

II. MATERIALS

The LIGA Ni samples with columnar microstructures were obtained from Sandia National Laboratories (Alberquerque, NM). The samples consisted of dog-bone-shaped Ni, fabricated by the LIGA process. This fabrication process involved electroplating Ni into PMMA molds that were realized by deep X-ray lithography. Electroplating was carried out in a sulfamate bath using a plating current density of 50 mA/cm^2. Further details on the LIGA process are given in References 1 and 2.

Y. YANG, Graduate Student, and W.O. SOBOYEJO, Professor, are with the Princeton Institute of the Science and Technology of Materials (PRISM), Princeton, NY, USA, and the Department of Mechanical and Aerospace Engineering, Princeton University, Princeton, NJ 08544, USA. Contact e-mail: soboyejo@princeton.edu S. ALLAMEH, Assistant Professor, is with the Department of Physics and Geology, Northern Kentucky University, Highland Heights, KY 41099, USA. J. LOU, Assistant Professor, is with the Department of Mechanical Engineering and Materials Science, Rice University, Houston, TX 77005, USA. B. IMASOGIE, Associate Professor, is with the Department of Metallurgical Engineering and Materials Science, Obafemi Awolowo University, Ile-Ife 220005, Nigeria. B.L. BOYCE, Principal Member of the Technical Staff, is with the Materials and Process Sciences Center, Sandia National Laboratories, Albuquerque, NM 87185, USA.

Manuscript submitted February 28, 2006.
Article published online August 10, 2007.

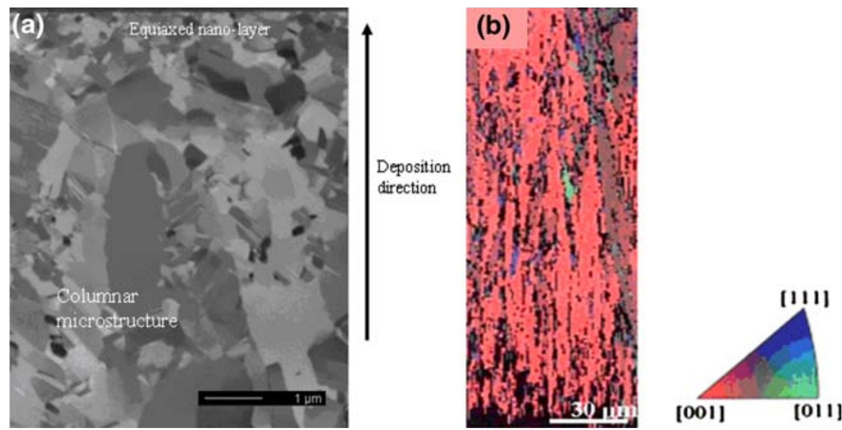

Fig. 1—Microstructure of LIGA Ni MEMS thin films: (*a*) FIB induced secondary electron image and (*b*) orientation microscopy image.

A focused ion beam (FIB) technique was used to reveal the microstructure (Figure 1(a)). This shows an initial seed layer of nanoscaled equiaxed grain structure (average grain size ~20 nm). It is important to note here that the nanoscaled grains correspond to the sidewall of the Ni structure grown in PMMA mold. Also, below this layer, the grain size increases with increasing distance from the deposition side, until it reaches a steady value of about 1 μm. Below this, the grain structure changes to a columnar structure with microscale features. The orientation microscopy image (Figure 1(b)) shows that the LIGA Ni thin film has a predominant {001} microtexture.

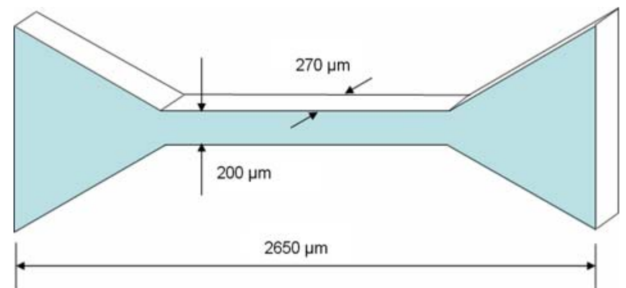

Fig. 2—Schematic of the dog-bone shape sample used for microtensile and microfatigue experiments.

III. EXPERIMENTAL PROCEDURES

A. *Microtensile Testing*

Microtensile tests were performed on the dog-bone specimens. The tests were carried out under displacement control, using an Instron model 5848 microtester (Instron, Canton, MA). The specimens were deformed continuously to failure at a strain rate of 5×10^{-4} s^{-1}. The local strains/displacements were monitored using an *in-situ* video camera with a 3000 × 4000 pixel resolution. The incremental images of gage section deformation and the loads were monitored with an automated image acquisition system.

B. *Microfatigue Testing*

The LIGA fatigue samples had the same dog-bone shape as the microtensile samples, as shown in Figure 2. The two triangular ends were used to secure the sample in the grips of the microtester. The distance between the two ends was 1200 μm, of which the middle 400 μm corresponded to the gage section with a uniform width of 200 μm. The dog-bone shape samples had a thickness of 270 μm. The samples were tested using a table top Instron (model 5848) microtester equipped with a 50 N load cell. The alignment of the gripping blocks and the loading of the samples were done with a traveling monoscope that was attached to a video monitoring system.

The tests were performed under load control at a cyclic frequency of 10 Hz with a load ratio $R = 0.1$. The load and cross-head displacement data were recorded continuously along with the number of cycles to failure.

C. *Fatigue Crack Growth Testing*

The fatigue crack growth tests were performed on LIGA Ni compact tension (CT) and single edge notched tension (SENT) specimens. The specimen configurations are shown in Figure 3. Before the tests, fatigue precracking was done at a stress intensity factor range of ΔK between 10 and 12 MPa$\sqrt{\text{m}}$ and a load ratio of $R = 0.1$. This was used to generate a sharp crack tip. Load shedding was then applied to reduce the possible retardation effect due to an enlarged crack-tip plastic zone.

During the fatigue test, both specimens were constrained in an antibuckling jacket. The actual fatigue crack growth test was carried out on an Instron model 5848 microtester. The test was conducted at a cyclic load with a frequency of 10 Hz. Crack growth was monitored continuously using a Questar telescope (Questar Inc., New Hope, PA) equipped with an image acquisition system and an electronic positioning system.

For the CT specimen, the test was continued until the fatigue crack size reached about 65 pct of the sample width. The specimen was then fractured and examined in a scanning electron microscope. For the SENT

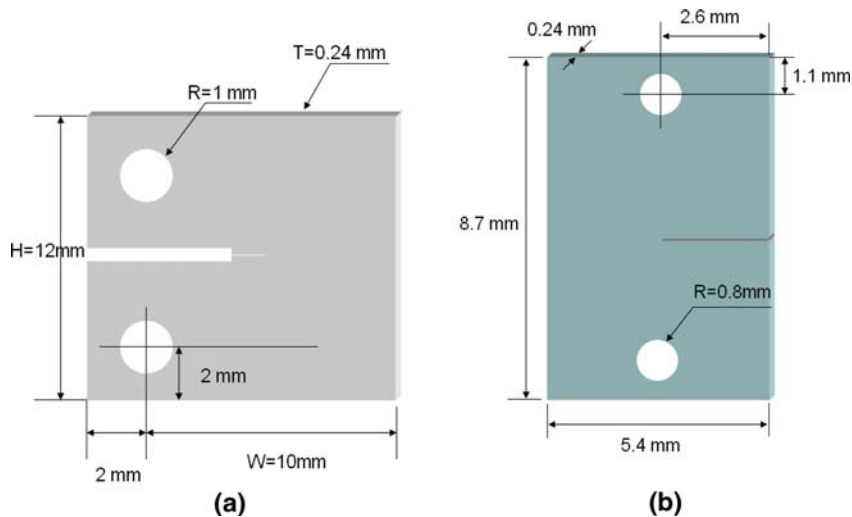

Fig. 3—Sketch of (*a*) the LIGA Ni CT specimen and (*b*) SENT specimen.

specimen, the test was stopped when the fatigue crack size was about 50 pct of the sample width. The specimen was then examined using the dual-beam focused ion beam and scanning electron microscopy (FIB/SEM) system (FEI Company, Hillsboro, OR) at Princeton University.

For the SENT specimen, the fatigue crack wake and tip configuration after load shedding are shown in Figure 4. As the fatigue crack advanced from the notch root and interacted with the material structure, a tortuous crack wake was left behind, as shown in Figure 4. Near the fatigue crack tip, surface microcracks were found. In order to reveal the underlying fatigue crack growth/fatigue crack-microstructure interactions, a FIB cut was made ahead of the fatigue crack tip.

For the FIB cut, a 1-μm-thick Pt sacrificial layer was first deposited at the place of interest (shown as the dashed line in the inset of Figure 4). The Ga^+ ion beams were then used to etch out a microsized pit, with the dashed line in Figure 4 being one of the pit edges. The specimen holder was then rotated from the ‘‘cutting’’ position, which was perpendicular to the incident ion beam, to a ‘‘scanning’’ position, which formed an angle of 52 deg with the incident ion beam, such that subsurface microstructure can be revealed due to an ‘‘ion channeling’’ effect when scanned by low intensity ion beams.

IV. EXPERIMENTAL RESULTS

A. *Microtensile Behavior*

The microtensile data obtained from the tests on the 270-μm-thick samples are presented in Figures 5(a) and (b). These include both engineering and true stress-strain curves. The true stress-strain curve (Figure 5(b)) reveals that the 270-μm-thick film has a 0.2 pct offset yield

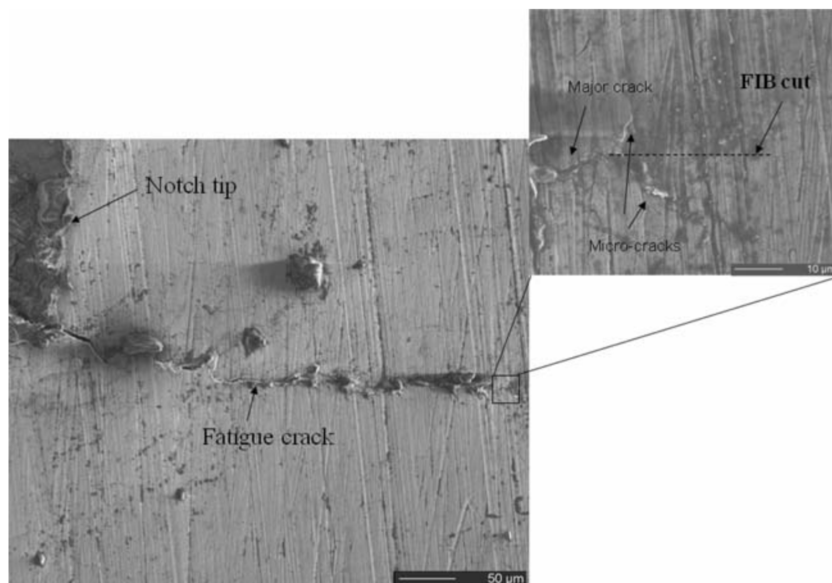

Fig. 4—Fatigue crack generated from the notch in a SENT specimen.

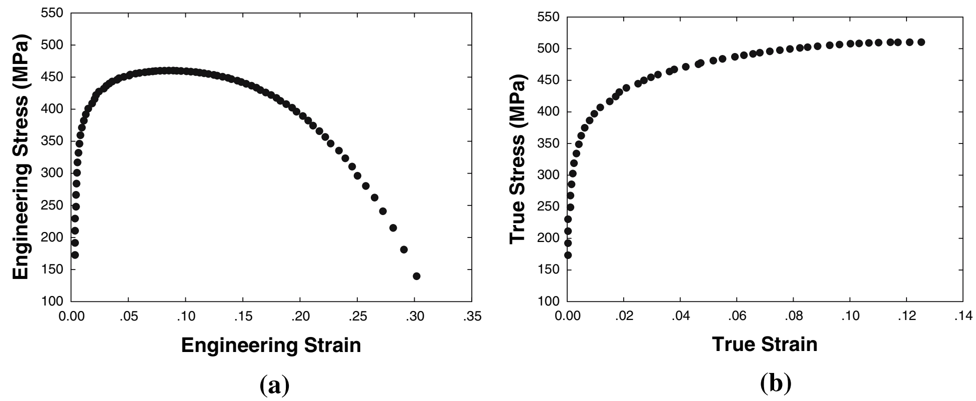

Fig. 5—Stress-strain curves obtained for LIGA Ni thin film: (*a*) engineering stress *vs* engineering strain and (*b*) true stress *vs* true strain.

Table I. Comparison of LIGA Ni Properties with Bulk Ni

Study	Thickness (μm)	0.2 Pct Offset Yield Strength (MPa)	Ultimate Tensile Strength (MPa)	Young's Modulus (GPa)
Current study	270	~340	~510	~170
Hemker and Last[9]	100 to 200	~360	~537	~180
Mazza *et al.*[15]	120 to 200	~405	~782	~202
Boyce *et al.*[34]	250	~304	~494	—
Sharpe *et al.*[41]	200	~323	~555	~176
Xie *et al.*[27]	200	~400	~540	~175
Lou *et al.*[18]	50	~385	~497	~189
	100	~475	~587	—
	200	~450	~547	—
Cho *et al.*[5]	300	~370	~ 544	~163
Bulk Ni[40]	—	59	317	207

stress of 305 MPa. The material also exhibits significant hardening, and the ultimate tensile strength is 500 MPa, which is significantly greater than the 0.2 pct offset yield stress. The Young's modulus of the 270-μm-thick film was determined to be ~170 GPa. This is comparable to prior reports by Cho *et al.*,[5] Mazza *et al.*,[15] Hemker and Last,[9] Lou *et al.*,[26] Xie *et al.*,[27] and Sharpe *et al.*,[41] as shown in Table I. For the 0.2 pct offset yield stress and ultimate tensile strength, the reported values for LIGA Ni thin films are much larger than those of bulk Ni.

B. *Fatigue Stress-Life Behavior*

The results of fatigue experiments are presented in Figure 6. The results are compared with the previously obtained fatigue data for bulk Ni in annealed and hardened conditions[5,42] and LIGA Ni MEMS data reported by Cho *et al.*[5] In the case of the 270-μm-thick columnar LIGA Ni samples, the fatigue endurance limit of the sample (taken at a fatigue life over 10^7 cycles) was about 210 MPa. This is in agreement with the findings of Boyce *et al.*,[34] who showed test runout (fatigue lives greater than 10^7 cycles) at a stress level of ~208 MPa and a stress ratio $R = -1$ in bending. This is also close to the fatigue endurance limit reported for bulk-annealed Ni.[5]

The ratio of the fatigue endurance limit to the ultimate tensile strength (endurance ratio) is about

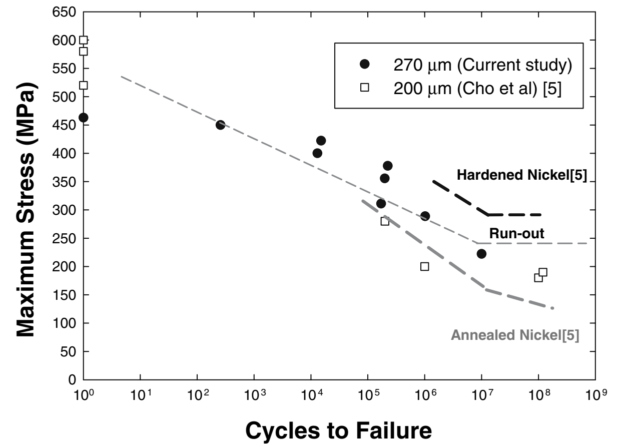

Fig. 6—Stress life data for the 270-μm-thick LIGA Ni thin film at $R = 0.1$.

45 pct for the 270-μm-thick LIGA Ni MEMS films with a columnar microstructure.[2,34] The results of this study are also consistent with the results of Cho *et al.*,[3,4,5] who tested LIGA Ni samples with comparable thickness (~200 μm). However, the latter results show lower endurance limits than those reported by Mohr *et al.* for Ni films (~10 μm).[16]

A power-law relationship between the applied stress amplitude and the fatigue life is used subsequently to

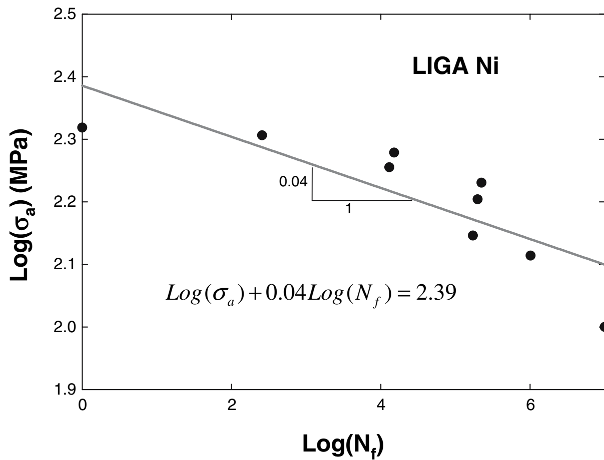

Fig. 7—Linear dependence of the logarithm of stress amplitude on the logarithm of fatigue life for LIGA Ni thin film.

characterize the stress life behavior obtained for the columnar LIGA Ni thin films. This empirical expression is given by[43]

$$\sigma_a = \beta (N_f)^\alpha \quad [1]$$

where σ_a is the stress amplitude, N_f is the number of cycles to failure, and α and β are material constants.

Figure 7 shows the linear relation between the logarithm of stress amplitude and the logarithm of fatigue life. From linear regression analysis, α and β are found to be –0.04 and 243. The results are comparable to the results from Cho.[5] Table II also lists the fatigue parameters for Si thin films.[43] It is of interest to note that the fatigue endurance limit for different thin films can be estimated from Eq. [1]. The fatigue endurance limits are evaluated at the fatigue stress life of 10^7. The results are compared in Table II, showing that the endurance limits of LIGA Ni thin films are one order of magnitude smaller than those of Si thin films.

C. *Fatigue Crack Nucleation and Short Crack Growth*

In an effort to identify the crack nucleation mechanisms in the LIGA Ni thin film, the gage sections of the microfatigue specimens were monitored in incremental stages using SEM images of the surface and subsurface regions that were revealed *via* FIB methods. The tests were also stopped at intervals corresponding to different fractions of the measured failure lives. Following each incremental loading stage (corresponding to $0.05N_f$, $0.1N_f$, $0.2N_f$ ... N_f), the gage sections of the deformed samples were imaged in a scanning electron microscope. These did not reveal evidence of surface-induced deformation up to ~80 to 90 pct of fatigue lives.

Surface or corner cracks were generally observed to nucleate within the gage sections of the fatigue specimens at about 80 to 90 pct of the fatigue lives. These are shown in Figures 8(a) through (c), in which the images of the deformed and cracked gage sections are presented for a 270-μm-thick columnar sample that was deformed for 1.5×10^6 cycles at a stress range of 259 MPa. Clear evidence of edge crack nucleation is observed at the sides of the specimen (Figures 8(a) and (c)), presumably as a result of stress concentration. Surface crack nucleation also occurs in the middle of the specimen (Figures 8(a) and (b)), with the fatigue cracks extending 10 to 20 μm across the width of the specimen.

It is of interest to examine the subsurface morphology of the nucleated cracks that were observed at the surfaces of the specimens (Figures 9(a) and (b)). This was revealed by examining the crack morphologies on the fracture surfaces using the SEM. The SEM images showed that the initiated cracks had classical semielliptical profiles with faceted crystallographic morphologies (Figure 9(a)). Subsequent early crack growth beyond this regime occurred by transgranular crack growth mechanisms, as shown in Figure 9(b). Further details on the "long" fatigue crack growth mechanisms will be presented in Section D using results obtained from tests on CT specimens.

D. *Long Fatigue Crack Growth*

The long fatigue crack growth data obtained from the CT specimen are presented in Figure 10. The logarithmic plot of da/dN against ΔK exhibits a sigmoidal variation, as in most engineering alloys.[42,47] The Paris power-law relationship, showing a linear variation of log da/dN with log ΔK, pertains to stable fatigue crack growth from about 8 to 32 MPa$\sqrt{\text{m}}$. This can be written as follows:

$$\frac{da}{dN} = 3.7 \times 10^{-8} (\Delta K)^{2.2} (\text{mm/cycle}) \quad [2]$$

For bulk Ni, the Paris law relationship is expressed as[50]

$$\frac{da}{dN} = 4 \times 10^{-9} (\Delta K)^{3.3} (\text{mm/cycle}) \quad [3]$$

where ΔK is the mode I stress intensity factor range. The subscript I is dropped for simplicity. (The same convention applies in the rest of this article except in

Table II. Summary of Fatigue Parameters

Material	Specimen	Film Thickness (μm)	α	β (MPA)	Predicted Fatigue Endurance Limit (MPA)
LIGA Ni thin films	Current study	270	–0.04	243	283
	Cho *et al.*[5]	200	–0.06	251	204
Si thin films	Kapel *et al.*[43]	4	–0.03	3000	4000
	Sharpe *et al.*[43]	3.5	–0.01	1000	2000

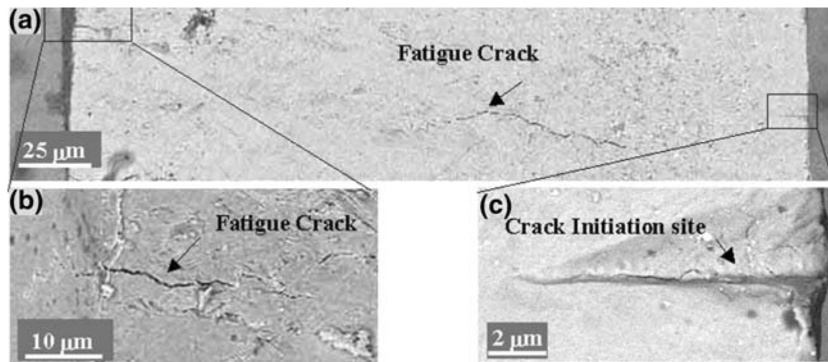

Fig. 8—Crack nucleation in 270-μm-thick LIGA Ni MEMS thin film deformed at a stress level of 259 MPa for 1.5×10^6 cycles: (*a*) fatigue crack initiated on the top surface, (*b*) fatigue crack nucleated at the corner of the sample, and (*c*) crack initiation site at the corner of the sample. Specimen failed after 3,251,900 cycles.

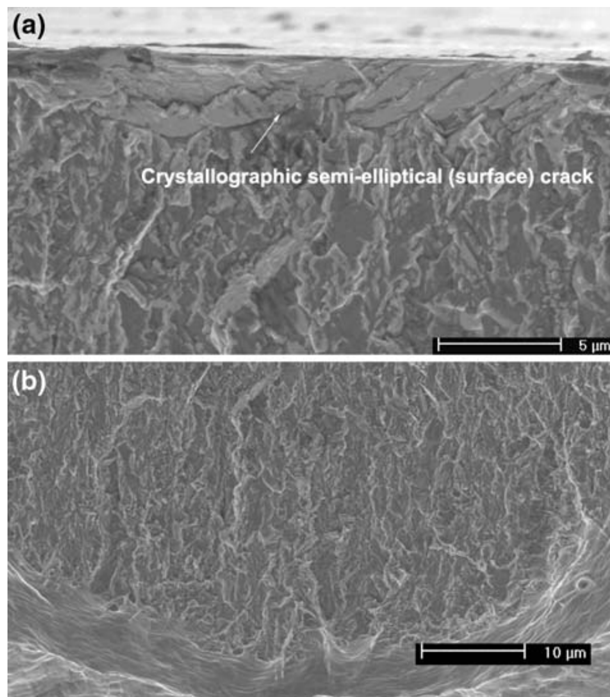

Fig. 9—SEM images of the cross section of fractured sample due to fatigue: (*a*) faceted crystallographic morphology at the crack nucleation site and (*b*) transgranular morphology in the long crack region.

cases where mixed mode loading is involved and the specific modes are defined explicitly). It is of interest to compare the crack growth behavior described by Eqs. [2] and [3] on the same plot. As is shown in Figure 10, LIGA Ni exhibits a greater crack growth resistance, and hence slower crack growth rates than bulk Ni in the intermediate ΔK regime, *i.e.*, from 8 to $32\text{MPa}\sqrt{\text{m}}$. The data obtained for LIGA Ni show that fatigue crack growth rates are generally slower than those in bulk Ni at the same ΔK levels in the Paris regime.

Figure 11 reveals the microstructure changes associated with long fatigue crack growth in LIGA Ni thin

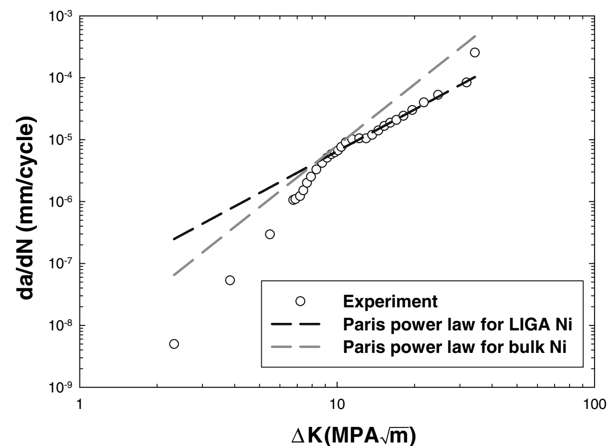

Fig. 10—Fatigue crack growth curve for LIGA Ni.

films. Similar phenomena were observed on two different specimens. This was revealed by digging a FIB pit ahead of the crack tip. Hence, the underlying microstructure reveals the microstructural changes that occur due to cyclic deformation ahead of the crack tip. In Figure 11(a), a recrystallized grain is formed near the surface on the left-hand side. This grain is over 10 times larger than the normal columnar grains. Within the recrystallized grain, microvoids were observed along with the surface and intergranular microcracks in the deformed columnar grains (Figure 11(b)).

The current results, therefore, suggest that fatigue crack growth is associated with dynamic recrystallization and deformation processes that give rise to microvoid formation and surface/subsurface intergranular crack growth during fatigue. Further work is needed to determine the details of how such processes give rise to stable fatigue crack growth in LIGA Ni MEMS thin films. These are clearly the challenges for future work.

The fatigue fracture modes are presented in Figures 12(a) through (c). In the near-threshold regime, a rough faceted crystallographic fracture mode was observed with a high incidence of secondary cracking (Figure 12(a)). This was followed by the Paris regime in

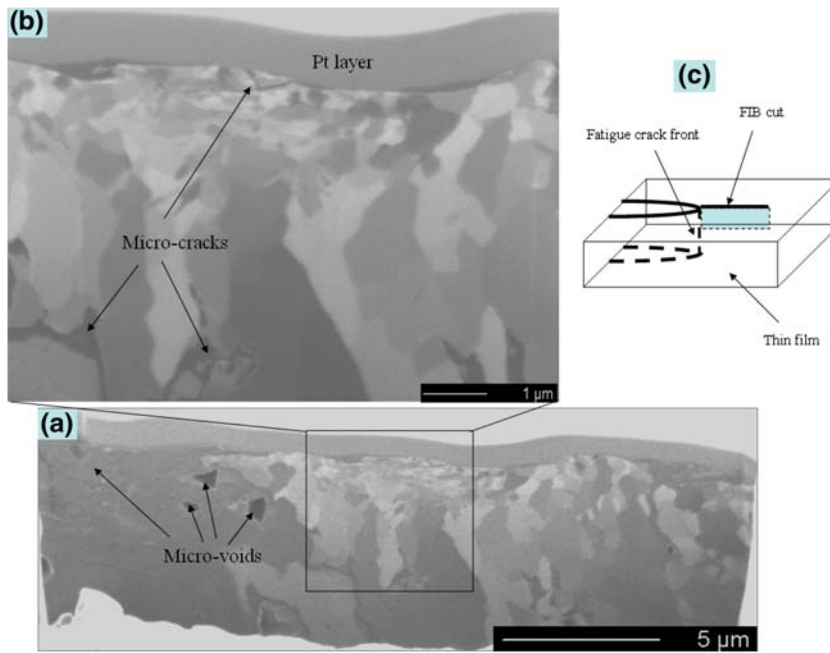

Fig. 11—The fatigue crack/microstructure interaction revealed by FIB: (*a*) recrystallized and deformed columnar grains and microvoids ($\Delta K \sim 10$ MPa$\sqrt{\text{m}}$), (*b*) surface and intergranular microcracks, and (*c*) schematic illustration of three-dimensional FIB cut orientation relative to the fatigue crack front.

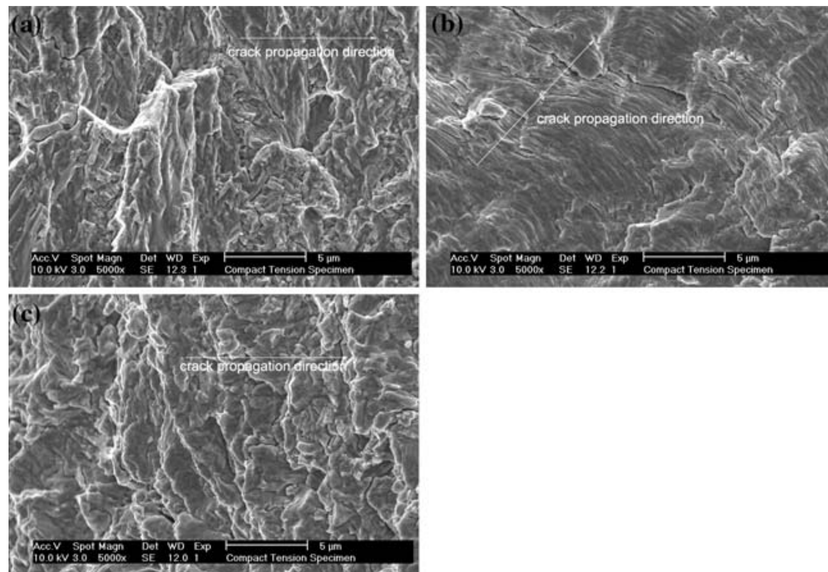

Fig. 12—Fracture modes at different ΔK regimes: (*a*) near-threshold ΔK regime, (*b*) intermediate ΔK (Paris law) regime, and (*c*) high ΔK regime.

which fatigue striations were observed (Figure 12(b)). As in conventional metals and their alloys, the fatigue striation spacing increased with the increasing stress intensity factor range, ΔK. Subsequently, a rough striated fatigue fracture mode was observed at higher ΔK values, and the incidence of secondary cracking increased with increasing ΔK (Figure 12(c)).

Before closing this section, it is of interest to examine the crack-tip shielding mechanisms that were revealed by the side images of the CT specimens. These revealed clear evidence of crack-tip shielding by crack deflection (Figure 13(a)), crack branching (Figure 13(b)), crack deflection induced by oxide inclusions (Figure 13(c)), and secondary cracking (Figure 13(d)), which can result in crack-tip shielding or antishielding.[42,47] Hence, the observed crack growth resistance is attributed, at least partly, to the shielding contributions from these mechanisms, as well as the intrinsic crack-tip plasticity associated with fatigue crack extension mechanisms.[42,47]

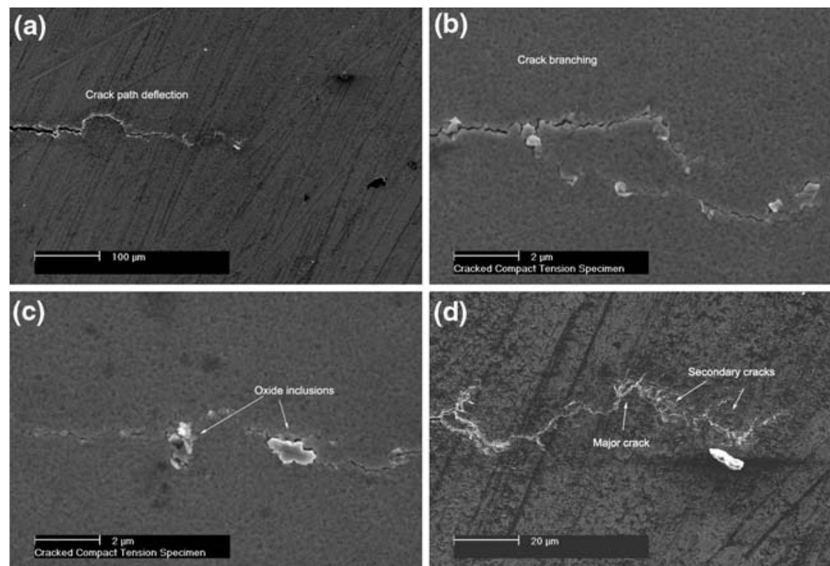

Fig. 13—Crack-tip shielding mechanisms in LIGA Ni thin film: (*a*) crack deflection, (*b*) crack branching, (*c*) crack deflection induced by oxide inclusion, and (*d*) microcracking.

V. DISCUSSION

The implications of the current work are quite significant. First, the stress-life experiments and the observations of crack nucleation suggest that crack nucleation occupies a significant fraction up to ~80 and 90 pct of the fatigue life at the stress levels used in this work. This corresponds to the number of cycles required to nucleate a 10-μm crack. Hence, the fraction of the fatigue life expended in the crack growth regime may be limited. Significant efforts are, therefore, needed to improve our fundamental understanding of the dislocation interactions and possible oxide-assisted phenomena[34] that can give rise to crack nucleation. These are clearly challenges for future work.

Before closing, it is of interest to note that the nanoscale grains on top of the columnar structure offer the potential for improving the overall fatigue life. This is because the small nanoscale grains are more likely to improve the resistance to fatigue crack nucleation, while the larger columnar grains are more likely to increase the resistance to fatigue crack growth.[42,47] However, further work is needed to establish the stability of the nanostructured layer of grains observed in the as-deposited microstructure. Further work is also needed to develop a basic understanding of the effects of microstructure on the nucleation and growth of fatigue cracks in LIGA Ni MEMS structure.

In any case, it is clear that the fatigue behavior of the current microstructure is dominated by crack nucleation phenomena in high-cycle fatigue. Because such phenomena are difficult to model at present, an empirical stress-life approach is recommended currently for fatigue life prediction. The crack growth resistance can also be ranked using the so-called long fatigue crack growth data. However, it is important to note that such data do not reflect possible short crack anomalies[42,47] that can occur during the early stages of fatigue crack growth. Further work is clearly needed to establish short crack growth rate data and the possible short crack anomalies that can occur in LIGA Ni MEMS thin films.

VI. CONCLUSIONS

The article presents the results of a study of fatigue in a LIGA Ni MEMS thin film with nanoscale grains on top of a columnar grain structure. The salient conclusions arising from this study are as follows.

1. The stress-life behavior is comparable to that reported previously for bulk-annealed Ni. The material exhibits an endurance limit of ~210 MPa, which corresponds to 45 pct of the tensile strength. Also, the initiation lives correspond to ~80 to 90 pct of the total fatigue lives.
2. The microscopic observations suggest that slip band formation is associated with fatigue crack nucleation. The nucleated cracks have nearly thumbnail/semielliptical or corner crack morphologies with faceted crystallographic morphologies.
3. The fatigue crack growth rate data are slower than prior reported data for annealed bulk Ni in the Paris regime. The Paris exponent of 2.2 is also smaller than the Paris exponent of 3.3 for bulk annealed Ni.
4. The FIB/SEM images of crack/microstructure interactions suggest that dynamic recrystallization occurs in the fatigue process zone. There is also evidence of microvoid formation and intergranular cracking in the fatigue process zone. This suggests a fatigue mechanism in which coupled deformation and mass transport processes result in cyclic damage in evolving microstructures in the vicinity of the crack tip.
5. The fatigue crack growth rate data exhibit three distinct regimes that are associated with characteristic

mechanisms. In the near-threshold regime, a rough crystallographic fatigue fracture mode is observed in fractography, while fatigue crack growth in the Paris regime involves fatigue striations. Finally, in the high ΔK regime, a rough striated fatigue fracture mode is observed along with a high incidence of secondary cracks.

ACKNOWLEDGMENTS

This research was supported by the Division of Materials Research, National Science Foundation (Grant No. DMR 0231418). Appreciation is extended to the Program Manager, Dr. Carmen Huber, for her encouragement and support. The authors also thank Dr. Tom Buchheit for providing the microscale columnar films that were used in the microtensile and stress-life fatigue experiments.

REFERENCES

1. T.E. Buchheit, T.R. Christenson, D.T. Schmale, and D.A. LaVan: *Mater. Res. Soc. Symp. Proc.*, 1999, vol. 546, pp. 121–26.
2. T.E. Buchheit, D.A. Van La, J.R. Michael, T.R. Christenson, and S.D. Leith: *Metall. Mater. Trans. A*, 2002, vol. 33A, pp. 539–54.
3. H.S. Cho, W.G. Babcock, H. Last, and K.J. Hemker: *Mater. Res. Soc. Symp. Proc.*, 2001, vol. 657, pp. EE5231–EE5236.
4. H.S. Cho, K.J. Hemker, K. Lian, and J. Goettert: *MEMS 2002 IEEE Int. Conf.*, 15th IEEE Int. Conf. on Micro Electro Mechanical Systems, IEEE, Piscataway, NJ, 2002, pp. 439–42.
5. H.S. Cho, K.J. Hemker, K. Lian, J. Goettert, and G. Dirras: *Sens. Actuat. A: Phys.*, 2003, vol. 103 (1–2), pp. 59–63.
6. T.R. Christenson, T.E. Buchheit, D.T. Schmale, and R.J. Bourcier: *Mater. Res. Soc. Symp. Proc.*, 1998, vol. 518, pp. 185–90.
7. J.C. Fox, R.L. Edwards, and W.N. Sharpe, Jr.: *Exp. Techniq.*, 1999, vol. 23 (3), pp. 28–30.
8. K.J. Hemker, H.S. Cho, Y. Desta, K. Lian, L.K. Jian, and J. Goettert: *HARMST-2001*, Baden-Baden, Germany, 2001.
9. K.J. Hemker and H. Last: *Mater. Sci. Eng. A*, 2001, vols. 319–321, pp. 882–86.
10. H. Jin, E.C. Harvey, J.P. Hayes, M.K. Ghantasala, A. Dowling, M. Solomon, and S.T. Davies: *Proc. SPIE: Int. Soc. Opt. Eng.*, 2001, vol. 4592, pp. 166–71.
11. H. Last, K.J. Hemker, and R. Witt: *Mater. Res. Soc. Symp. Proc.*, 2000, vol. 605, pp. 191–97.
12. J. Lou, P. Shrotriya, S. Allameh, N. Yao, T. Buchheit, and W.O. Soboyejo: *Mater. Res. Symp. Proc.*, 2001, vol. 687, pp. 41–46.
13. H. Majjad, S. Basrour, P. Delobelle, and M. Schmidt: *Sens. Actuat. A: Phys.*, 1999, vol. 74 (1–3), pp. 148–51.
14. C.K. Malek and L. Thomas: *Proc. SPIE*, 2000, vol. 4019, pp. 484–91.
15. E. Mazza, S. Abel, and J. Dual: *Microsyst. Technol.*, 1996, vol. 2, pp. 197–202.
16. J. Mohr and M. Strohrmann: *J. Micromech. Microeng.*, 1992, vol. 2, pp. 193–95.
17. F. Munnik, F. Benninger, S. Mikhailov, A. Bertsch, P. Renaud, H. Lorenz, and M. Gmur: *Microelectr. Eng.*, 2003, vols. 67–67, pp. 96–103.
18. J. Lou, S. Allameh, T. Buccheit, and W.O. Soboyejo: *J. Mater. Sci.*, 2003, vol. 38, pp. 4129–35.
19. W.N. Sharpe, Jr. and A. McAleavey: *Proc. SPIE Int. Soc. Opt. Eng.*, 1998, vol. 3512, pp. 130–37.
20. W.N. Sharpe, Jr., D.A. LaVan, and R.L. Edwards: *Proc. Int. Conf. Solid-State Sens. Actuat.*, 1997, vol. 1, pp. 607–10.
21. P. Shrotriya, S.M. Allameh, J. Lou, T.E. Buchheit, and W.O. Soboyejo: *Mech. Mater.*, 2003, vol. 35, pp. 223–43.
22. D. Sparks, D. Slaughter, R. Beni, L. Jordan, M. Chia, D. Rich, J. Johnson, and T. Vas: *Sens. Mater.*, 1999, vol. 11, pp. 197–207.
23. D.R. Sparks and S.C. Chang: *Proc. SPIE Int. Soc. Opt. Eng.*, 1997, vol. 3223, pp. 218–22.
24. L.S. Stephens, K.W. Kelly, S. Simhadri, A.B. McCandless, and E.I. Meletis: *J. Microelectromech. Syst.*, 2001, vol. 10, pp. 347–59.
25. M. Strobel, U. Schmidt, K. Bade, and J. Halbritter: in *Electrochemical Nanotechnology. In-Situ Local Probe Techniques at Electrochemical Interfaces*, W.J.P. Lorenz, ed., Wiley-VCH, Weinheim, Germany, 1998, pp. 215–24.
26. M. Strobel, U. Schmidt, K. Bade, and J. Halbritter: *Microsyst. Technol.*, 1996, vol. 3, pp. 10–16.
27. Z.L. Xie, D. Pan, H. Last, and K.J. Hemker: *Mater. Res. Soc. Symp. Proc.*, 2000, vol. 605, pp. 197–202.
28. M. Zupan and K.J. Hemker: *Exper. Mech.*, 2002, vol. 42, pp. 214–20.
29. M. Madou: *Fundamentals of Microfabrication*, 2nd ed., CRC Press, New York, NY, 2002.
30. *Reliability, Testing, and Characterization of MEMS/MOEMS III*, Proc. SPIE International Society of Optical Engineers, D.M. Tanner and R. Ramesham, eds., 2003, vol. 5343, pp. 235–43.
31. S.M. Allameh, J. Lou, F. Kavishe, T.E. Buchheit, and W.O. Soboyejo: *Mater. Sci. Eng. A*, 2004, vol. 371, pp. 256–66.
32. D.R. Sparks, M.I. Chia, and S. Zarabadi: in *Reliability of Resonant Micromachined Sensors and Actuators*, SAE Inc., Warrendale, PA, 2001, pp. 1–10.
33. D.R. Sparks, M.I. Chia, and G.Q. Jiang: *Sens. Actuat. Phys.*, 2001, vol. 95, pp. 61–68.
34. B.L. Boyce, J.R. Michael, and P.G. Kotula: *Acta Mater.*, 2004, vol. 52, pp. 1609–19.
35. W.N. Sharpe, Jr., S. Brown, G.C. Johnson, and W. Knauss: in S. Brown, J. Gilbert, H. Guckel, R. Howe, G. Johnson, P. Krulevitch, and C. Muhlstein, eds., *Round-robin Tests of Modulus and Strength of Polysilicon. Microelectromech. Struct. Mater. Res.*, MRS, San Francisco, CA, 1998, pp. 57–65.
36. W.N. Sharpe Jr.: in *Size Effects on Mechanical Properties of Polysilicon, ASME*, Mater. Div. (Publ.), MD, 1998, vol. 84, pp. 153–55.
37. C. Ioannis and W.G. Knauss: in C.R. Friedrich, and Y. Vladimirsky, eds., "Mechanical Properties of Thin Polysilicon Films by Means of Probe Microscopy. Materials and Device Characterization" in *Micromachining. Proc. SPIE*, 1998, vol. 3512, pp. 66–75.
38. R. Ballarini, R.L. Mullern, H. Kahn, and A.H. Heuer: *Proc. Microelectromech. Struct. Mater. Res.*, MRS Spring Meeting, San Francisco, CA, 1998, vol. 518, pp. 137–42.
39. S. Jarayaman, R.L. Edwards, and K.J. Hemker: *J. Mater. Res.*, 1999, vol. 14, pp. 688–97.
40. K. Lian, J. Jiang, Z.G. Ling, and E.I. Meletis: *Proc. SPIE.*, 2003, vol. 4980, pp. 192–99.
41. W.N. Sharpe Jr, D.A. LaVan, and R.L. Edwards: *Proc. Int. Solid State Sens. Actuators Conf.*, IEEE, New York, NY, USA, 1997, vol. 601, pp. 607–10.
42. W.O. Soboyejo: *Mechanical Properties of Engineered Materials*, Marcel Dekker, New York, 2003.
43. K. Bhalerao, A.B. Soboyejo, and W.O. Soboyejo: *J. Mater. Sci.*, 2003, vol. 38, pp. 4157–62.
44. R. Hertzberg: *Deformation and Fracture Mechanics of Engineering Materials*, 4th ed., John Wiley, 1996.
45. M. Ciappa and W. Fichtner: *Proc. IEEE Int. Reliability Phys. Symp.*, 2000, vol. 38, pp. 210–16.
46. S.D. Antolovich and A. Saxena: in *ASM Handbook*, 5th ed., ASM International, 1995, pp. 104–05.
47. S. Suresh: *Fatigue of Materials*, 2nd ed., Cambridge University Press, UK, 1999.
48. P. Shrotriya, S.M. Allameh, and W.O. Soboyejo: *Mech. Mater.*, 2004, vol. 36, pp. 35–44.
49. C.L. Muhlstein and R.T. Ritchie: *Mech. Mater.*, 2004, vol. 36, pp. 13–33.
50. D. Roylance: *Mechanics of Materials*, John Wiley & Sons, New York, NY, 1996.